Geological Society of America
Special Paper 385
2005

Historical earthquakes of the Puerto Rico–Virgin Islands region (1915–1963)

Diane I. Doser*
Christina M. Rodriguez
Claudia Flores
Department of Geological Sciences, University of Texas at El Paso, El Paso, Texas 79968-0555, USA

ABSTRACT

We have collected and modeled the seismograms of historic earthquakes of M >6.0 occurring in the Puerto Rico and Virgin Islands region between 1915 and 1963. Study of offshore events in the north Mona Passage region indicate likely rupture along the North America plate interface in 1915 (M_W = 6.7), 1920 (M_W = 6.5), and 1943 (M_W = 7.8 and 6.0) at depths of 20–30 km. (M_W is moment magnitude.) An event in 1917 (M_W = 6.9) involved strike-slip faulting possibly within the subducting North America plate (36 ± 7 km). The 1918 central Mona Passage earthquake (M_W = 7.2) represents normal-oblique faulting at ~20 km depth. This earthquake generated a tsunami that killed over 100 people on the island of Puerto Rico. The event has a complex source-time function, suggesting rupture along several fault segments. This is consistent with previous tsunami modeling studies. An event in 1916 in southeastern Hispaniola (M_W = 6.8) occurred at a depth of ~16 km, with a reverse faulting mechanism similar to aftershocks of the 1946 great Hispaniola earthquake. Within the Virgin Islands region, we studied three moderate (M ~6–6.5) events. An event in 1930 (M_W = 6.0) appears to involve strike-slip faulting, possibly within the subducting North America plate, while events in 1919 and 1927 (M_W = 6.2 and 5.6) are consistent with rupture along the plate interface. An event in 1939 (M_W = 6.4), located well to the north of the Puerto Rico trench, appears to be a normal faulting event in the outer rise. Slip vectors for earthquakes along the plate interface show northeastward directed slip (~50°) of the Greater Antilles crust relative to the North America plate in the Virgin Island region, north-northeast (~27°) directed slip in the northeast Mona Passage (east of 67.5°W), and east-northeast (~70°) directed slip in the northwest Mona Passage. Normal faulting events in the Greater Antilles crust suggest southeast-northwest oriented extension. Over the past ~85 yr, 87% of the seismic moment release has occurred on structures to the north and northwest of Puerto Rico. This is comparable to estimates of the amount of plate motion that is occurring across these structures from global positioning system and geodesy studies.

Keywords: Puerto Rico–Virgin Islands, historic earthquakes.

*E-mail, Doser: doser@geo.utep.edu. Present addresses: Rodriguez—Exxon-Mobil Corp., Houston, Texas, USA; Flores—University of California at Santa Cruz.

Doser, D.I., Rodriguez, C.M., and Flores, C., 2005, Historical earthquakes of the Puerto Rico–Virgin Islands region, *in* Mann, P., ed., Active tectonics and seismic hazards of Puerto Rico, the Virgin Islands, and offshore areas: Geological Society of America Special Paper 385, p. 103–114.

INTRODUCTION

The Puerto Rico–Virgin Islands region is located within a zone of complex, oblique subduction (Fig. 1) between the North America and Caribbean plates. East and south of the Puerto Rico–Virgin Islands region, trench normal subduction of North America beneath the Caribbean plate occurs along the Lesser Antilles arc. West of the Puerto Rico–Virgin Islands region, the buoyant Bahamas Platform sits upon the North America plate. The platform resists subduction, causing a transition to transform motion along the northern boundary of the Caribbean plate (e.g., Dolan et al., 1998). Both global positioning system (GPS) results (Jansma et al., 2000) and recent earthquake focal mechanisms (e.g., Deng and Sykes, 1995) indicate left-lateral oblique shortening is occurring north of the Puerto Rico–Virgin Islands region along the Puerto Rico trench (Fig. 1).

Subduction also occurs south of Puerto Rico along the Muertos trough (Fig. 1), with the Caribbean plate thrust beneath the Greater Antilles crust (e.g., Dillon et al., 1994). This leads to active collision between the Caribbean and Atlantic lithospheric slabs beneath eastern Hispaniola and the Mona Passage (Dillon et al., 1994; Dolan et al., 1998). Recent GPS (Jansma et al., 2000) and focal mechanism studies (Huerfano, 1995) suggest there is also a significant component of left-lateral strike-slip motion across the trough. The Muertos trough appears to die out within the southern Virgin Islands (Fig. 1) near 65°W (Masson and Scanlon, 1991).

The Mona Passage (Fig. 1) separates the Puerto Rico–Virgin Islands region from Hispaniola. Structures observed on the seafloor of Mona Passage (Larue and Ryan, 1990; van Gestel et al., 1998) suggest recent, east-west oriented extension within the central Mona Passage. Modeling of tsunami run-ups generated by the 1918 central Mona Passage earthquake (Mercado and McCann, 1998), as well as focal mechanisms of recent earthquakes, indicates normal faulting is presently occurring within the central Mona Passage.

The Anegada Passage forms the southeastern boundary of the Puerto Rico–Virgin Islands region (Fig. 1). It appears to be a zone of left-lateral transtension that transfers displacement from the eastern edge of the Muertos trough to the Puerto Rico trench (Masson and Scanlon, 1991; Jansma et al., 2000).

Thus, the Puerto Rico–Virgin Islands region is sandwiched between four seismogenic zones: the Puerto Rico trench to the north, the Muertos trough to the south, the Mona Passage to the west, and the Anegada Passage to the southeast (Fig. 1). This complex tectonic setting has produced numerous large to great earthquakes, although most have occurred prior to 1963, and thus little is known about the relationship between these events and the regional tectonics.

In order to study the earthquakes of the Puerto Rico–Virgin Islands region, we have divided the region into two areas, based on the clustering of historic and recent events (Fig. 2). The first region (Figs. 4 and 5), located primarily west and northwest of Puerto Rico, is dominated by seismicity associated with the Puerto Rico trench and strike-slip faults within the Greater Antilles crust (Septentrional fault, North Puerto Rico Slope fault, South Puerto Rico Slope fault). The region is located at the eastern edge of the rupture zone of the 1946 great (M_W = 8.0) Hispaniola earthquake (Dolan and Wald, 1998) and includes the source regions of the 1943 (M_W = 7.8) North Mona Passage earthquake (Dolan and Wald, 1998) and the 1787 (M = 8–8¼) Puerto Rico trench earthquake (McCann, 1985) (Fig. 2).

Eastern Puerto Rico and the Virgin Islands form the second study area (Figs. 6 and 7). This region is the site of the 1867 (M_S = 7.5) Anegada Passage earthquake (McCann, 1985) (Fig. 2). Most recent seismicity occurs within the northern portion of the study area. McCann and Sykes (1984) suggest that the seismicity clustered between 64°W and 65°W is caused by the subduction of an aseismic ridge that can be followed to the northwest along strike to the position of the Main Ridge (Fig. 1) within the unsubducted North America plate.

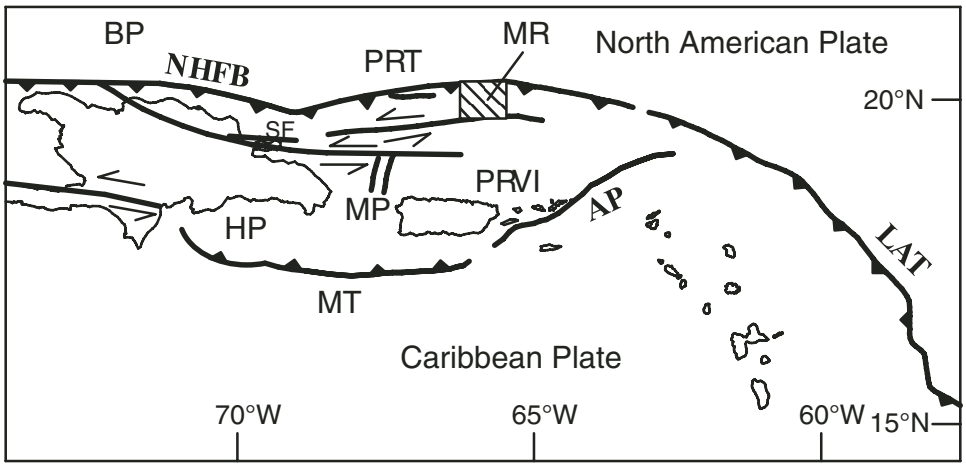

Figure 1. Map of the Puerto Rico–Virgin Islands study area showing major tectonic features modified from Jansma et al. (2000). AP—Anegada Passage; BP—Bahamas Platform; HP—Hispaniola platelet; LAT—Lesser Antilles trench; MP—Mona Passage; MR—Main Ridge; MT—Muertos trough; NHFB—northern Hispaniola fold belt; PRT—Puerto Rico trench; PRVI—Puerto Rico–Virgin Islands block; SF—Septentrional fault

ANALYSIS TECHNIQUES

The earthquakes we have selected for analysis are listed in Table 1. In order to obtain adequate, high quality body-wave information at teleseismic distances, we restricted our study to M >5.9 earthquakes occurring after 1914 and prior to 1964 when the establishment of global seismograph networks allowed for more routine analysis of moderate to large magnitude earthquakes. Within the Puerto Rico–Virgin Islands region, the most recent M >5.9 earthquake occurring prior to 1964 was an aftershock of the 1943 North Mona Passage sequence (Table 1).

Locations for our earthquakes are taken from Russo and Bareford (1993) and Russo (1995, personal commun.). The relocations used a technique similar to that described in Russo and Villaseñor (1995) using the location technique of Wysession et al. (1991) and Russo et al. (1992). Error ellipses were not given for the earthquakes; however, standard deviations in predicted versus observed arrival times for the earthquakes are given in Table 1.

Although we did not have access to the complete phase data set used by Russo and Bareford (1993) and Russo (1995, personal commun.), we did relocate the 1918 central Mona Passage event and the 1920 North Mona Passage event using the iterative bootstrap relocation technique of Petroy and Wiens (1989). Error ellipses for these relocations are shown in Figure 2, and suggest that the uncertainties in the locations of the oldest events (pre-1930, when worldwide seismograph station coverage was very poor) could be as much as 50 km.

Our waveform modeling technique uses the inversion method of Baker and Doser (1988), which inverts body waveforms for focal mechanism, focal depth, and source-time function shape. First motion data, mapped surface faults, focal mechanisms of recent earthquakes and surface wave magnitudes, when available, are used to estimate a priori source parameter values and their associated uncertainties from the

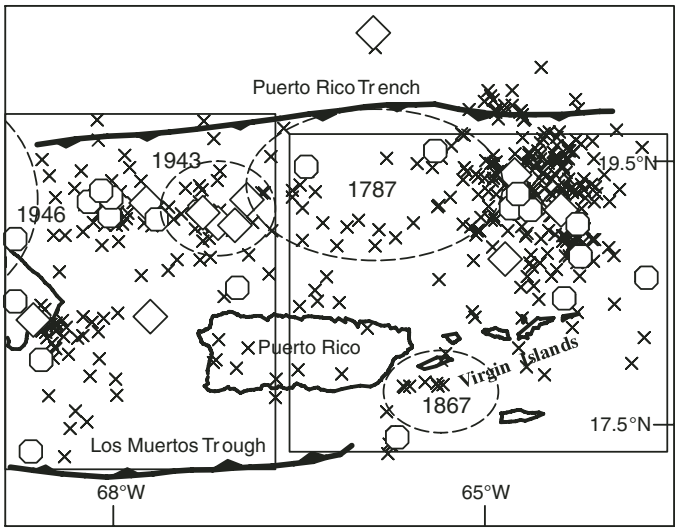

Figure 2. Approximate rupture zones of historic earthquakes (dashed lines) from McCann (1985) and Dolan and Wald (1998), recent seismicity (x's) (NEIC catalog magnitude >3.9 from 1973 to 2001), earthquakes of this study (diamonds) (Table 1), and recent M_W > 4.8 earthquakes (octagons) (Table 2). The boxes indicate the northwestern offshore Puerto Rico and Virgin Islands study areas described in the text and shown in Figures 4 and 6.

TABLE 1. SOURCE PARAMETERS OF HISTORIC EARTHQUAKES

Date (mo/d/yr)	Time	Location* (lat–long)	s.d.* (sec)	Focal mechanism (strike, dip, rake)	Slip† vector (deg)	Depth (km)	M_o §	M_W #	M**
101115	1933	19.04–67.10	4.2	85, 40, 55††	50	20††	4.5††	6.4	6¾
042416	0426	18.26–68.53	3.1	281 ± 38, 50 ± 10, 105 ± 20	9	16 ± 7	19 ± 3	6.8	6¾
072717	0101	19.16–67.66	3.3	65 ± 28, 80 ± 17, –170 ± 13	—	36 ± 7	22 ± 4	6.9	7
101118	1414	18.28–67.62	3.7	207 ± 22, 54 ± 8, –127 ± 28	170	20 ± 7	64 ± 7	7.2	7½
090619	0604	19.36–64.77	3.9	153, 40, 80††	65	30††	2.4††	6.2	6¼
021020	2207	19.07–67.28	3.1	65 ± 40, 30 ± 21, 50 ± 20	20	27 ± 7	5.7 ± 2	6.5	6½
080227	0051	19.10–64.43	2.8	317, 84, 122††	47	20††	0.5††	5.6	6½
062530	1206	18.72–64.87	2.9	167, 87, 168††	—	50††	1††	6.0	6¼
061239	0405	20.41–65.90	2.3	310, 65, –120††	—	10††	1.5††	6.4	6¼
072943	0302	18.99–66.97	2.7	50 ± 21, 30 ± 16, 30 ± 24	23	29 ± 3	529 ± 30	7.8	7¾
				60, 20, 60§§		>25§§	—	7.9§§	
073043	0102	19.17–66.86	2.0	60 ± 40, 30 ± 17, 45 ± 30	18	24 ± 3	1.1 ± 0.2	6.0	6½

*Locations and standard deviations (s.d.) from Russo and Bareford (1993) and R.M. Russo (personal commun., 1995).
†See text for description of how fault plane was selected. Slip vectors were not calculated for events within the subducting North America or Caribbean plates.
§Seismic moment in N-m × 10^{18}.
#Moment magnitude.
**Magnitude from Gutenberg and Richter (1954).
††Results from forward modeling.
§§Results from Dolan and Wald (1998).

TABLE 2. SOURCE PARAMETERS OF RECENT EARTHQUAKES

Date (mo/d/yr)	Time	Location (lat–long)	Focal mechanism (strike, dip, rake)	Slip vector* (deg)	Depth (km)	M_w†	Reference§
052363	0743	19.10–64.78	188, 80, –90	—	50	—	MS
081064	0110	19.03–67.28	168, 82, –100	—	48	5.2 (m_b)	MS
110366	1624	19.17–67.93	94, 39, 9	85	23	5.6	SB
012279	0425	19.10–64.64	75, 14, 28	46	22	5.3	CMT
031579	0658	18.87–68.69	348, 41, 62	—	93	5.0	CMT
110579	0151	17.96–68.46	93, 22, 87	—	78	6.2	CMT
021480	1711	18.43–64.38	138, 17, 82	55	55	4.9	CMT
061182	2157	18.74–64.25	105, 48, 27	85	42	5.1	CMT
093082	1335	18.59–63.76	155, 36, 116	33	37	5.0	CMT
092083	0851	18.39–68.67	50, 43, 64	—	96	5.4	CMT
062685	1710	19.25–64.73	90, 29, 18	73	27	5.9	CMT
072185	1310	19.12–68.11	76, 23, 14	62	23	5.6	CMT
110388	1942	19.04–67.58	63, 38, 0	63	37	5.9	SB
061889	1406	17.28–68.53	34, 64, –22	—	73	5.4	CMT
112392	0631	18.51–66.96	224, 43, –64	110	15	5.3	CMT
080193	1932	17.42–65.71	267, 28, –57	140	15	5.3	CMT
051196	0218	19.54–65.41	143, 39, 134	0	27	5.1	CMT
120898	0232	18.98–64.27	215, 50, –126	125	15	5.4	CMT
121100	1854	19.41–66.40	174, 50, 135	25	15	5.4	CMT
101601	1527	19.31–64.88	40, 18, –24	62	15	5.6	CMT
101701	1129	19.30–64.97	88, 24, 41	48	15	5.8	CMT

*See text for description of how fault plane was selected. Slip vectors were not calculated for events within the subducting North American or Caribbean plates.

†Moment magnitude, except for the 081064 earthquake, where body wave magnitude (m_b) is given.

§MS—Molnar and Sykes (1969); SB—Soto-Cordero and Bataille (1993); CMT—Harvard Centroid Moment Tensor catalog (www.seismology.harvard.edu/CMTsearch.html).

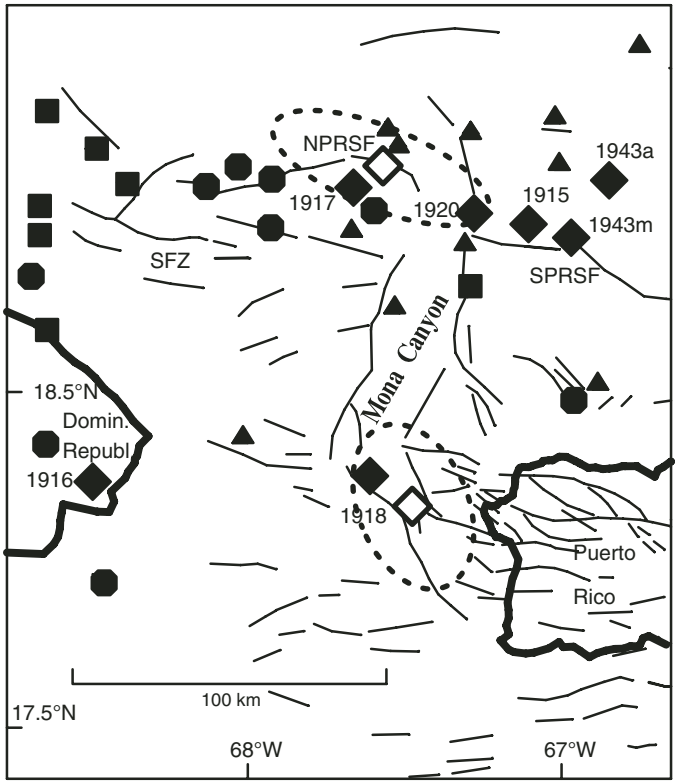

Figure 3. Historic and recent seismicity (M_w >4.8) of the northern offshore Puerto Rico region. Locations of historic events are from Russo and Bareford (1993) and R.M. Russo (1995, personal commun.). Dashed ovals and open symbols show 90% confidence ellipses and locations for the 1918 and 1920 earthquakes, respectively, obtained by using the relocation technique of Petroy and Wiens (1989). See text for details. Triangles are aftershocks of the 1943 North Mona Passage mainshock (labeled 1943m), squares are aftershocks of the 1946 great Hispaniola earthquake, diamonds are historic events of this study, and octagons are recent M_w >4.8 events (Table 2). SFZ—Septentrional fault zone; NPRSF—northern Puerto Rico slope fault zone; SPRSF—southern Puerto Rico slope fault zone.

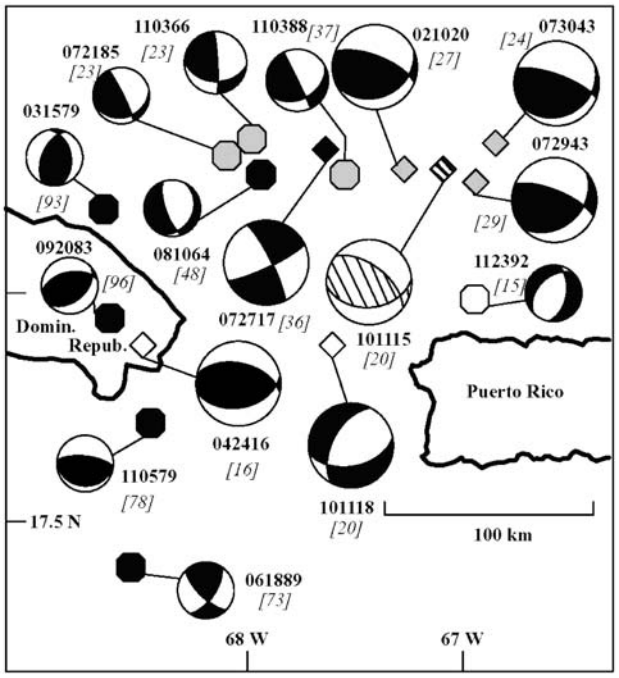

Figure 4. Focal mechanisms of northwestern offshore Puerto Rico earthquakes. Large mechanisms are from this study (Table 1); small mechanisms are for recent M_W >4.8 events (Table 2). Striped mechanisms were obtained from forward modeling studies and are less reliable. The italic numbers in brackets are focal depths. Black symbols are events below the plate interface, gray symbols are events on the plate interface, and open symbols are events above the plate interface. Striped symbols denote suspected plate interface events (based on focal mechanisms) whose depths are poorly constrained. See text for details. A north-south cross section along 67.75°W is shown in Figure 5.

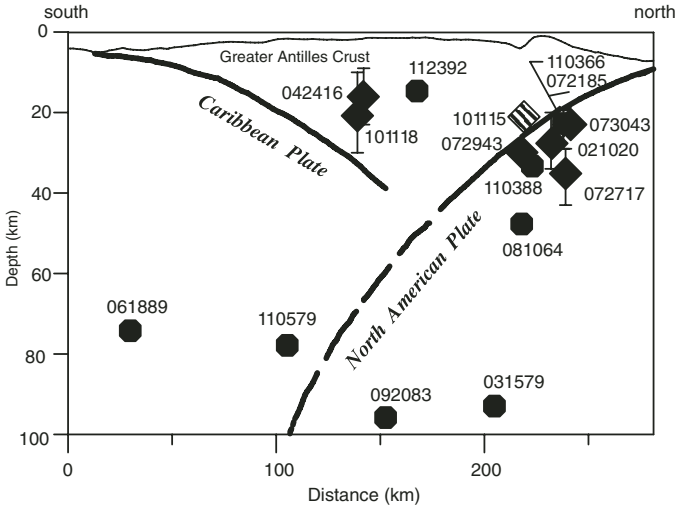

Figure 5. Cross section along 67.75°W showing the locations of the North America and Caribbean plate interfaces, modified from Dolan et al. (1998). Diamonds indicate historic events with error bars shown for results obtained from waveform inversions. Striped symbols denote more poorly constrained depths obtained from forward waveform modeling studies. Note vertical exaggeration.

inversion. Individual seismograms are weighted based on their observed signal to noise ratios and the uncertainties in instrument response parameters. Final covariances in the inversion are calculated using the maximum value of the misfit of the best solution or the initial covariances. These revised covariances result in an estimate of solution uncertainty (Table 1; Appendix, Figs. A1–A11) that is less likely to be biased by overly optimistic estimates of initial data or model quality or by restrictive a priori information (Baker and Doser, 1988). The uncertainties obtained using this inversion technique have been extensively compared to estimates from forward modeling and from other inversion techniques (e.g., Doser et al., 1999; Doser and Webb, 2003) and have generally been found to be more pessimistic than other techniques for describing source parameter uncertainties.

Layered near-source velocity models were built using the crustal velocity models of Huerfano (1995) combined with the structural cross sections of Dolan et al. (1998) to estimate depth to the plate interface. A water layer was also used in our models, since many events are located beneath 4–5 km of water.

Seismograms were hand-digitized. Each seismogram was corrected for mean and trend and resampled at a 0.5 s sampling rate.

Sufficient waveform data (normally 5–6 seismograms from a total of at least 3 stations) to conduct inversions for source parameters were not available for about half of the events. In these cases, as explained in the following sections, we conducted forward modeling studies of possible focal mechanisms for the earthquakes. The results from forward modeling are indicated by the striped focal mechanisms in Figures 4 and 6 and are also given in Table 1. The waveform fits and focal mechanism uncertainties are shown in the Appendix.

RESULTS

Northwestern Offshore Puerto Rico

Waveform analysis was conducted for seven events within the northwestern offshore region. Our analysis included the 1943 North Mona Passage mainshock. Dolan and Wald (1998) had previously studied this earthquake (Table 1), but have not published a complete, detailed account of their waveform modeling analysis procedures. They suggest both the 1943 North Mona Passage and 1946 Hispaniola earthquakes represent rupture along the North America plate interface at strongly coupled asperities associated with underthrusting of the Silver, Navidad, and Mona carbonate banks of the eastern Bahamas platform.

The focal mechanisms of historic and recent earthquakes are shown in Figure 4. Recent mechanisms (smaller size) were obtained from first motion or Centroid Moment Tensor (CMT) studies (see Table 2). The symbol color indicates suspected position relative to the plate interface (Fig. 5). All earthquakes falling within 10 km of the plate interface and having mechanisms

consistent with low angle slip along the interface were considered plate interface events. Striped mechanisms indicate poorly constrained mechanisms obtained from forward waveform modeling. Striped symbols indicate events with poorly constrained focal depths obtained from forward modeling.

The earliest event of our study occurred in 1915 and appears to be located west of the 1943 mainshock (Fig. 3). The sparse waveform data from two stations (Fig. A1) did not allow for waveform inversion studies of this event. We used forward modeling to test several possible strike-slip and dip-slip mechanisms (based on mechanisms of surrounding recent and historic events) for this earthquake. The waveforms are most consistent with rupture on a reverse or thrust fault with a focal mechanism similar to the nearby 1920 and 1943 earthquakes. The depth could not be constrained well enough to determine if the earthquake occurred on the plate interface (Fig. 5), but its similarity to other nearby interface events suggests it also may have occurred on the interface.

Inversion of waveform data for the 1916 southeastern Hispaniola earthquake suggests it occurred on a reverse fault within the Greater Antilles crust (Figs. 4, 5, and A2). Its mechanism is similar to some of the aftershocks of the 1946 great Hispaniola earthquake determined by Dolan and Wald (1998). The mechanism indicates continued compression and uplift within eastern Hispaniola due to the collision of the Caribbean and Atlantic slabs beneath this region.

The 1917 North Mona Passage earthquake is located in a region between the 1943 and 1946 aftershock zones (Fig. 3) where bathymetric data reveal a 7-km-deep pull-apart basin (Dolan et al., 1998). Dolan and Wald (1998) suggested the gap between the 1943 and 1946 rupture zones existed either because: (1) a recent earthquake (possibly the 1917 event) had occurred in the region and had relieved the strain along the plate interface, or (2) strain accumulation occurred more slowly along this portion of the plate interface due to a lack of asperities. Although several reverse faulting mechanisms were used as a priori starting models, the waveforms do not appear to be consistent with a reverse mechanism (see modeling results, Fig. A3). The best waveform fit was obtained for strike-slip mechanisms (Table 1; Fig. 4) at a depth of 36 ± 7 km, suggesting faulting within the subducting North America plate (Figs. 4 and 5). Thus, the 1917 earthquake does not appear to have relieved strain along the plate interface.

Of special interest to this study was analysis of the 1918 central Mona Passage earthquake. This earthquake generated a tsunami that struck the western coast of Puerto Rico, resulting in the loss of over 100 lives. Mercado and McCann (1998) modeled tsunami run-up heights for the earthquake, suggesting the earthquake occurred along a series of four normal faults striking 185°–235° with lengths of 4–31 km and displacements of 4 m. Our results are consistent with their multiple fault rupture model. The complexity and duration of the source-time function we obtain (Fig. A4) indicates slip along at least two fault patches, each ~18 km long with ~3 m average slip. The nodal plane striking 210° (Fig. 4) is most consistent with Mercado and McCann's modeling results. Limited first motion data from Vieques, Puerto Rico, and Seminaire Saint Martial, Haiti (Reid and Taber, 1919), are also consistent with this mechanism (Fig. A4).

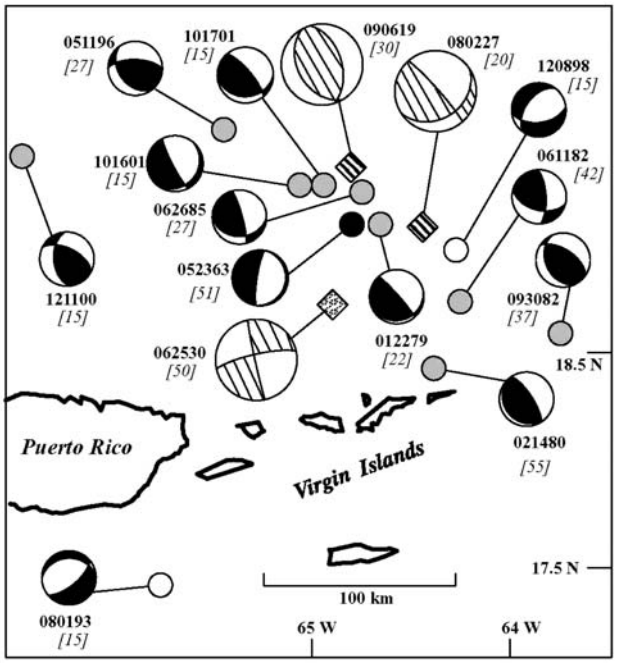

Figure 6. Historic and recent earthquakes of the Virgin Islands region. Large focal mechanisms denote historic earthquakes of this study (Table 1). The striped mechanisms indicate more poorly constrained mechanisms from forward modeling studies. Small focal mechanisms denote recent M_W >4.8 earthquakes (Table 2). Black symbols are events below the plate interface, gray symbols are events on the plate interface, and open symbols are events above the plate interface; the symbol filled with wavy lines denotes an event that is suspected to have occurred within the subducting North America plate. A north-south cross section along 65°W is shown in Figure 7.

Focal mechanisms and depths for the 1920 earthquake and the 1943 North Mona Passage mainshock and its largest aftershock are all consistent with rupture along the plate interface (Figs. 4, 5, A6, A10, and A11). Our results for the 1943 mainshock agree with those of Dolan and Wald (1998), although our best-fit mechanism has a slightly lower rake (Table 1). Dolan and Wald suggest that rupture in the 1943 mainshock propagated in the down-dip direction starting at a depth of ~25 km (comparable to our depth estimate of 29 ± 3 km) and that the lateral extent of the rupture zone was related to the collisional underthrusting of a portion of the Bahamas Bank (Mona Bank). This is consistent with the hypocentral location of the 1943 aftershock we studied (Fig. 5), which indicates the aftershock occurred well up-dip of the mainshock rupture. The hypocenter for the 1920 earthquake, although poorly constrained, also appears to be up-dip of the 1943 mainshock (Fig. 5) and located at the southwestern edge of the 1943 aftershock rupture zone (Fig. 3). Thus, the 1920 event may have relieved stress along the plate interface in this region and arrested continued westward rupture of the plate interface in 1943.

Virgin Islands Region

There were fewer large (M >5.9) earthquakes in the Virgin Island region than the Puerto Rico region during the twentieth century (Fig. 2), although the southwestern Virgin Islands experienced an M ~7.5 earthquake (McCann, 1985) in 1867. We studied three events in this region, as well as an event in 1939 located well to the north of the Puerto Rico trench (Fig. 2). Because these earthquakes were smaller than M = 6.5, very limited seismogram data were available. This required us to conduct forward modeling of the seismograms using a number of starting models for each event that were based on the focal mechanisms and depths of recent earthquakes located within 100 km of their epicenters.

Figure 6 shows focal mechanisms (smaller mechanisms) of recent events (Table 2) in comparison to the historic events. Striped focal mechanisms indicate events with poorly constrained mechanisms obtained from forward modeling studies. Striped symbols indicate events with focal depths poorly constrained by forward modeling, but with mechanisms consistent with rupture along the plate interface. The symbol with wavy lines indicates an event with a focal depth poorly constrained by forward modeling, but with a mechanism that is not consistent with rupture along the plate interface. Note that although the mechanism for earthquake 101601 appears to be normal-oblique (Table 2), only a slight change in the dip (<5°) of the more steeply dipping nodal plane would create a reverse-oblique mechanism similar to the neighboring earthquake on 101701. Thus, we have classified earthquake 101601 as a plate interface event.

A cross section of the region is shown in Figure 7. Again, all earthquakes falling within 10 km of the plate interface and having mechanisms consistent with low angle slip along the interface were considered interface events.

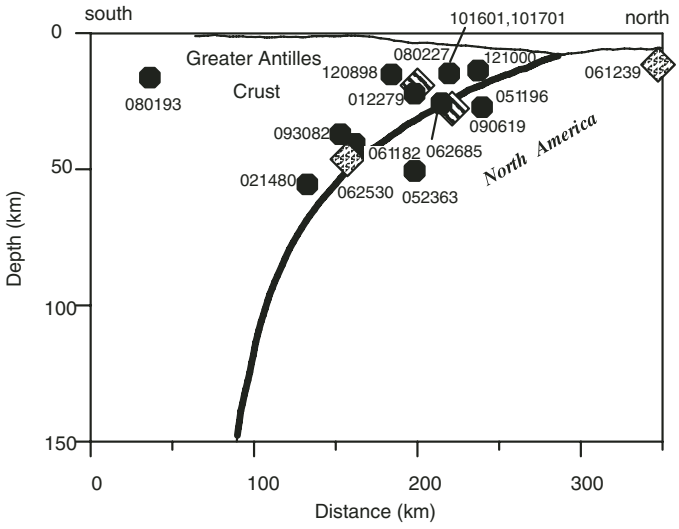

Figure 7. Cross section along 65°W showing the North America plate interface (modified from Dolan et al., 1998). Diamonds are historic events. The focal mechanism for the 1939 earthquake is shown in Figure 8. Symbols are as in Figure 6. Note vertical exaggeration.

Limited waveform data for the 1919 northern Virgin Islands earthquake (Fig. A5) suggest this event involved reverse/thrust faulting, possibly along the plate interface (Fig. 7). The 1927 earthquake is also consistent with reverse or thrust faulting along the plate interface (Figs. 6, 7, and A7), with a mechanism similar to that of the nearby June 1985 (M_W = 5.9) earthquake.

Waveform modeling suggests a strike-slip mechanism for the 1930 earthquake (Figs. 5 and A8). Reverse and normal faulting mechanisms similar to nearby recent earthquakes did not fit the observed P-wave first motion polarity at La Paz and grossly overestimated P-wave amplitudes at La Paz and DeBilt.

Forward modeling of waveform data for the 1939 earthquake (Fig. A9), located well north of the Puerto Rico trench (Fig. 2), gives a mechanism that suggests normal faulting within the North America plate at a depth of ~10 km (Fig. 7). Thus, this earthquake appears to be an outer rise event.

SLIP VECTORS AND SEISMIC MOMENT RATES

Slip vectors of events known or suspected to be located above the plate interface (i.e., within the Greater Antilles crust) (open symbols) or on the plate interface (gray or striped symbols) are shown in Figure 8 and given in Tables 1 and 2. Thin arrows indicate events with focal mechanisms that were more poorly resolved (i.e., from forward modeling studies). Striped symbols indicate events with poorly determined focal depths that we suspect occurred on the plate interface. The large arrow in Figure 8 indicates the average direction of motion of the Puerto Rico–Virgin Islands block relative to the North America plate (~17 mm/yr, N68°E) from the GPS studies of Jansma et al. (2000).

For reverse or thrust events of the Puerto Rico region (101115, 042416, 021020, 072943, 073043, 110366, 110388, 072185, 121100), we selected the southward dipping nodal plane as the fault plane, with slip vectors indicating the movements of the south blocks of the faults relative to the north blocks. Note that we grouped the 121100 event with other events in the Puerto Rico region since it is actually closer to the North Mona Passage events than the northern Virgin Island events (Fig. 8). In the case of known or suspected plate interface events, the slip vectors would thus represent the movement of Greater Antilles crust relative to the North America plate.

For normal faulting events on 101118 and 112392, we selected the northeast-southwest striking, northwest dipping nodal planes as the fault planes, with slip vectors indicating the motions of the southeastern fault blocks relative to the northwestern fault blocks. These nodal planes are the most consistent with mapped faults in the region. For the 1918 event, the selected nodal plane is also the nodal plane most consistent with the tsunami modeling studies of Mercado and McCann (1998).

The slip vectors from the reverse or thrust events suggest that in the northeastern Mona Passage motion of the Puerto Rico plate relative to North America is directed toward the north-northeast

(an average of 27° for the 5 interplate events located between 66°W and 67.5°W). There is a rotation of slip along the interface to ~70° west of 67.5°W (average of 3 events). This rotation of slip to a most westerly direction west of 67.5°W is consistent with the GPS studies of Mann et al. (2002) that suggest there is a change in the direction and rate of plate motion across the Mona Passage, from a most easterly strike (~80°) and slower rate (4–17 mm/yr) of plate motion within central and eastern Hispaniola to a strike of ~70° and rate of 19–20 mm/yr within the Puerto Rico–Virgin Islands region.

Slip vectors for events within the Greater Antilles crust show southwest to south-southwest directed extension within the central and eastern Mona Passage. The 1916 Hispaniola event shows possible northward directed slip along the thrust fault systems of eastern Hispaniola.

In the Virgin Islands region, we again selected the southward dipping nodal planes as the fault planes for the thrust or reverse events (090619, 080227, 012279, 021480, 061182, 093082, 062685, 051196, 101601, 101701), all of which are known or suspected plate interface events. The average slip vector for these ten events is northeast (50°), rotated ~20° counterclockwise of the motion of the Puerto Rico–Virgin Islands block relative to North America.

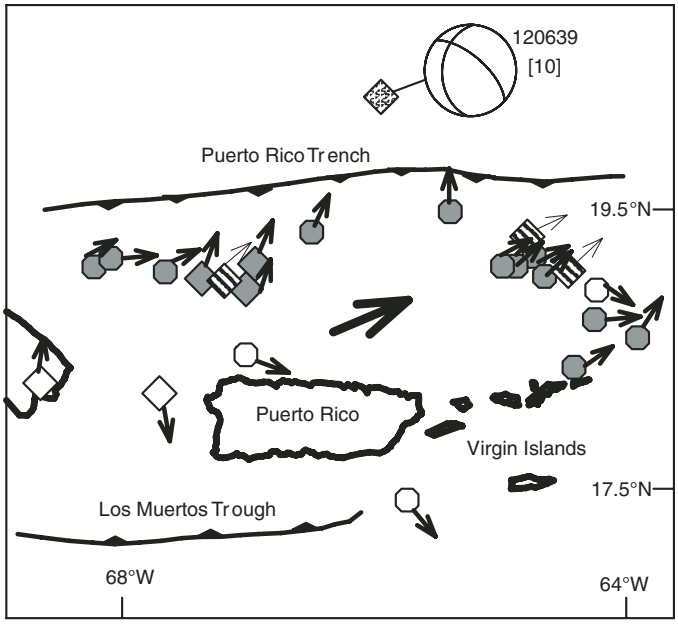

Figure 8. Slip vectors of earthquakes occurring in the upper plate (i.e., Greater Antilles crust) (open symbols) or along the plate interface (i.e., between the Greater Antilles crust and North America plate) (gray symbols). Striped symbols denote events with poorly constrained focal depths that are suspected to have occurred on the plate interface. Slip vectors are given in Tables 1 and 2. Small bold arrows denote events with better determined focal mechanisms. See text for a detailed description of how slip vectors were determined. The large bold arrow is the direction of motion of the Puerto Rico–Virgin Islands block relative to the North America plate (Jansma et al., 2000). The focal mechanism for the 1939 outer rise event (Table 1) is shown at top.

For the 080193 and 120898 normal faulting events, we selected the northwest dipping nodal planes as the fault planes. These gave slip vectors suggesting southeastward directed slip of the southeastern sides of the fault blocks, similar to that observed to the west within the Mona Passage.

The GPS and geodesy studies of Jansma et al. (2000) suggest that ~85% of North America–Caribbean plate motion takes place within the Puerto Rico trench and upon faults located north and northwest of Puerto Rico, with the remainder taken up to the south. This is in good agreement with estimates of seismic moment release over the past ~85 yr, with 87% of seismic moment release (Tables 1 and 2) occurring along structures located north and northwest of Puerto Rico. Another 13% of the seismic moment release took place within the Mona Passage region, where extension rates are estimated to be 2–5 mm/yr (Jansma et al., 2000).

Although offshore faults do not pose as much hazard to Puerto Rico as onshore faults, the effect of rupture directivity should not be overlooked. The 1943 mainshock appears to have ruptured to the west (Dolan and Wald, 1998) and down-dip, causing only intensity V shaking in Puerto Rico (Coffman and von Hake, 1982), and thus may not be representative of the "typical" shaking that could be expected from north Mona Passage events. The 1918 central Mona Passage earthquake, however, with rupture propagation upward to the surface as indicated by the tsunami modeling studies of Mercado and McCann (1998), produced intensity IX effects within Puerto Rico (Coffman and von Hake, 1982).

CONCLUSIONS

Studies of M > 5.9 historic earthquakes of the Puerto Rico–Virgin Islands region indicate that many historic events are consistent with slip along the plate interface, both in the northeastern Mona Passage and the Virgin Islands regions. Crustal deformation has been limited to the 1918 central Mona Passage and the 1916 eastern Hispaniola earthquakes. Focal mechanisms and focal depths for earthquakes in 1917 in the north Mona Passage and 1930 in the Virgin Islands region suggest strike-slip faulting, possibly within the subducting North America plate.

Slip vectors suggest north-northeast to east-northeast directed movement of the Greater Antilles crust relative to North America along the plate interface. The strike of slip appears to change most dramatically across the northern Mona Passage, a result consistent with recent GPS observations of marked differences in the rate and direction of relative plate motion across the Mona Passage.

Seismic moment release within the Virgin Islands region over the past ~85 yr has been nearly two orders of magnitude lower than that of the northwestern offshore Puerto Rico region. This is also consistent with GPS studies suggesting that the structures offshore of northwestern Puerto Rico accommodate ~85% of North America–Caribbean plate motion.

APPENDIX

In the following appendix figures, the observed seismograms are shown on top and the synthetic seismograms on the bottom of each seismogram pair. The labels below seismogram pairs refer to station code and waveform type (z = vertical P-waves, r = radial P-waves, sh = transverse S-waves). The vertical scale shows the amplitudes of the waveforms in centimeters. Seismogram labels with a slash (/) indicate seismograms have been reduced relative to the vertical scale by the given factor. Labels with asterisks indicate that seismograms have been magnified by the given factor relative to the vertical scale. The bold vertical lines above each observed seismogram indicate the start of the phase that was modeled.

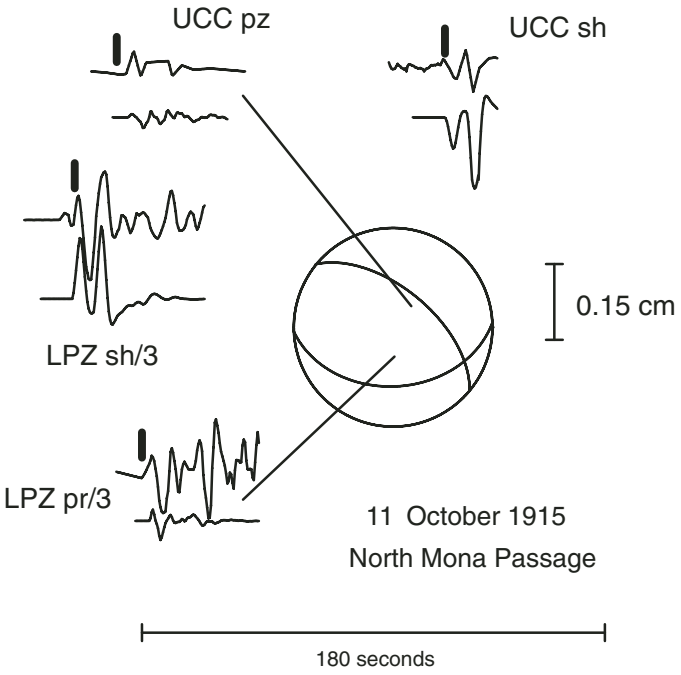

Figure A1. Waveform modeling results obtained from forward modeling of the 1915 North Mona Passage earthquake (see Table 1 and Fig. 4). LPZ—La Paz, Bolivia; UCC—Uccle, Belgium.

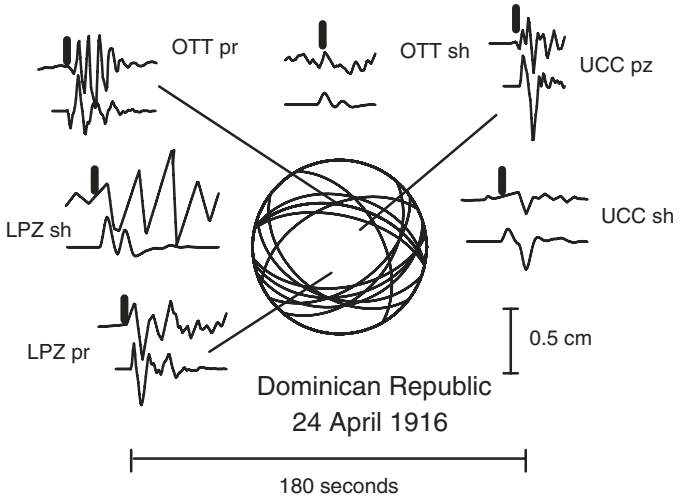

Figure A2. Results of waveform inversion for the 1916 Dominican Republic earthquake. The inversion results are given in Table 1. The range of focal mechanisms shown indicates the solution uncertainty (see Table 1). LPZ—La Paz, Bolivia; OTT—Ottawa, Canada; UCC—Uccle, Belgium.

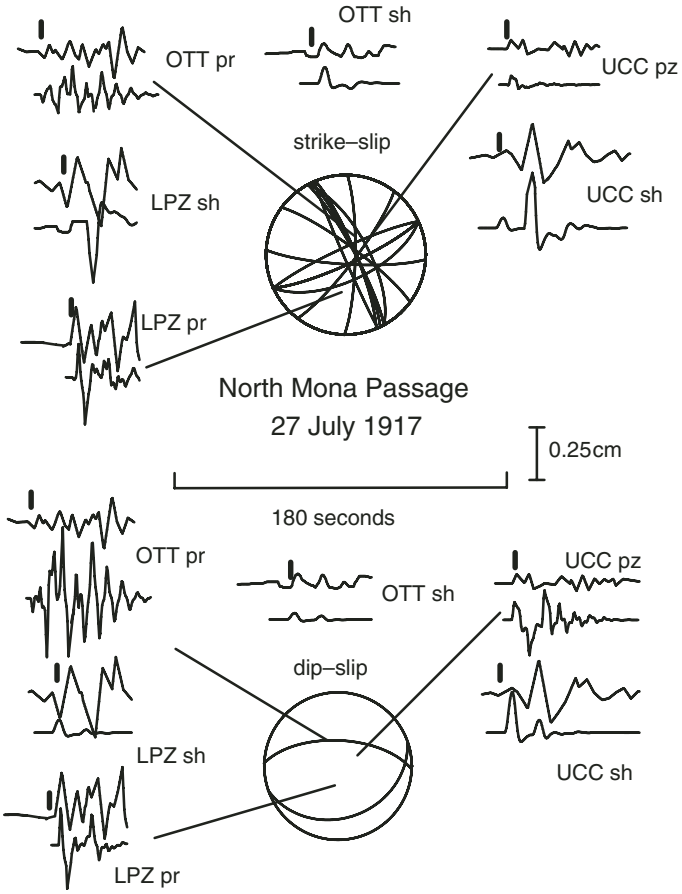

Figure A3. Results of waveform inversion for the 1917 North Mona Passage earthquake. The top synthetic seismograms were obtained for the strike-slip solution shown in Figure 4 and given in Table 1. The range of focal mechanisms shown reflects the uncertainty in the focal mechanism obtained from the inversion. The bottom seismograms were obtained for the dip-slip solution shown. Note that P-wave amplitudes are grossly overestimated at UCC and OTT, S-wave amplitudes are grossly overestimated at UCC, and the polarity of the S-wave at LPZ is mismatched for the dip-slip mechanism. The moment-magnitude of the event would have to be lowered to 6.6 (from 6.9) to obtain an amplitude match to the P-waves observed at UCC and OTT, although Gutenberg and Richter (1954) estimated the event to have a magnitude of 7.0 (Table 1). LPZ—La Paz, Bolivia; OTT—Ottawa, Canada; UCC—Uccle, Belgium.

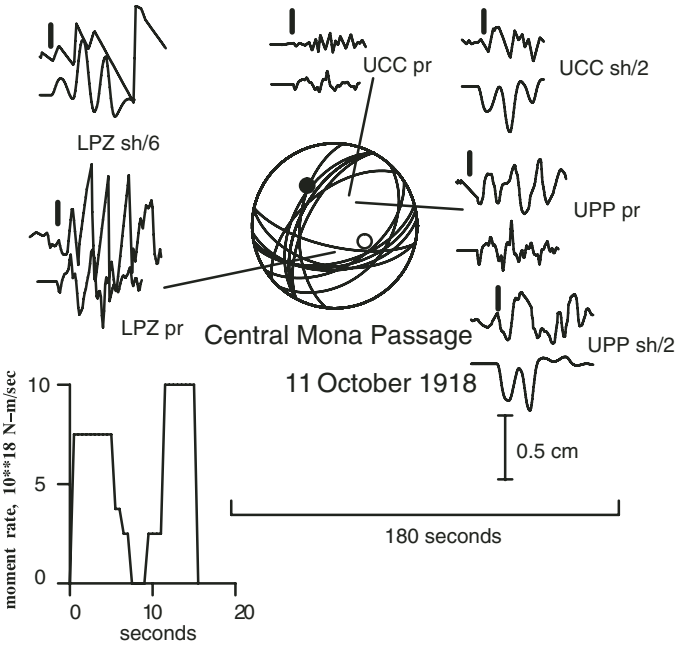

Figure A4. Results of waveform inversion for the 1918 central Mona Passage earthquake. The range of focal mechanisms shown reflects uncertainties obtained in the inversion process (Table 1). The source-time function shown at the lower left indicates the complex nature of the source rupture. The black symbol indicates the compressional first motion observed at Seminaire Saint Martial, Haiti, and the open symbol the dilatational first motion observed at Vieques, Puerto Rico (Reid and Taber, 1919). LPZ—La Paz, Bolivia; UCC—Uccle, Belgium; UPP—Uppsala, Sweden.

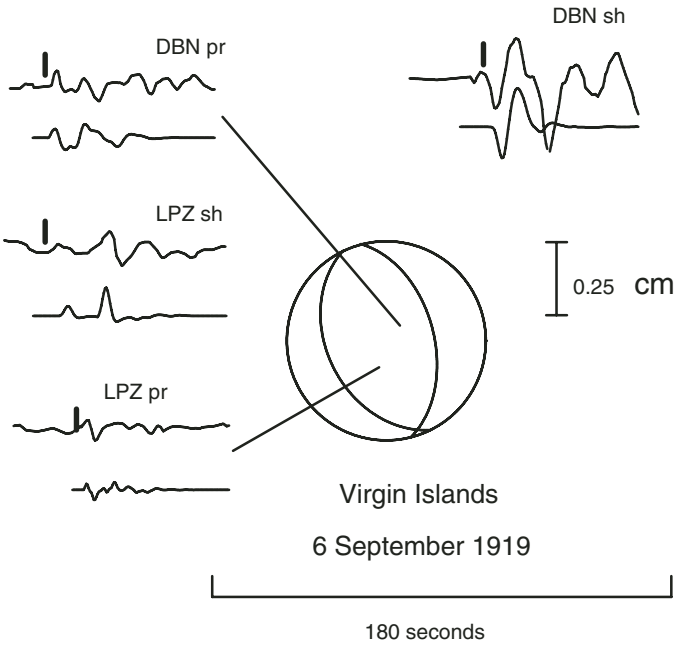

Figure A5. Results of forward modeling of the 1919 Virgin Islands earthquake. DBN—DeBilt, Netherlands; LPZ—La Paz, Bolivia.

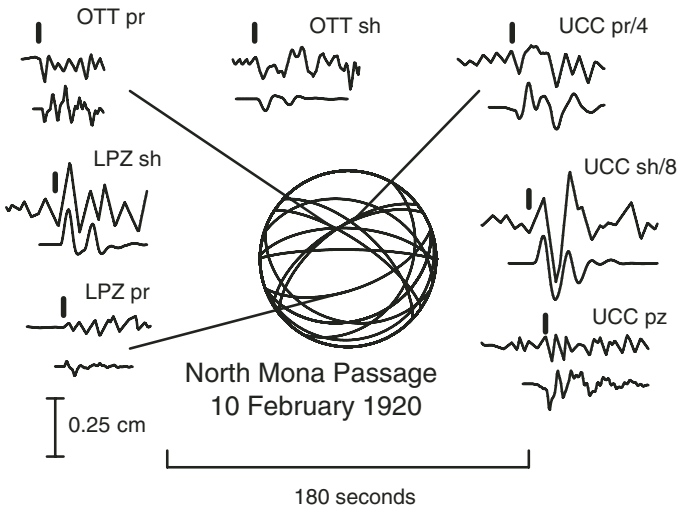

Figure A6. Results from the inversion of waveform data for the 1920 North Mona Passage earthquake. LPZ—La Paz, Bolivia; OTT—Ottawa, Canada; UCC—Uccle, Belgium.

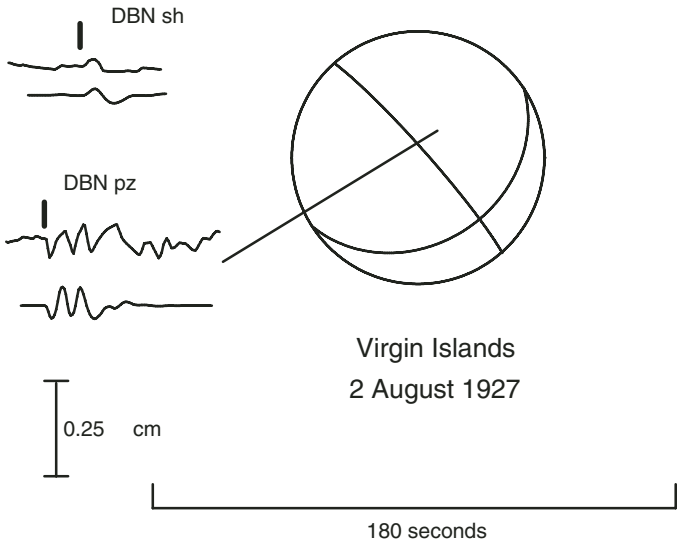

Figure A7. Results obtained from forward modeling of the 1927 Virgin Islands earthquake. DBN—DeBilt, Netherlands.

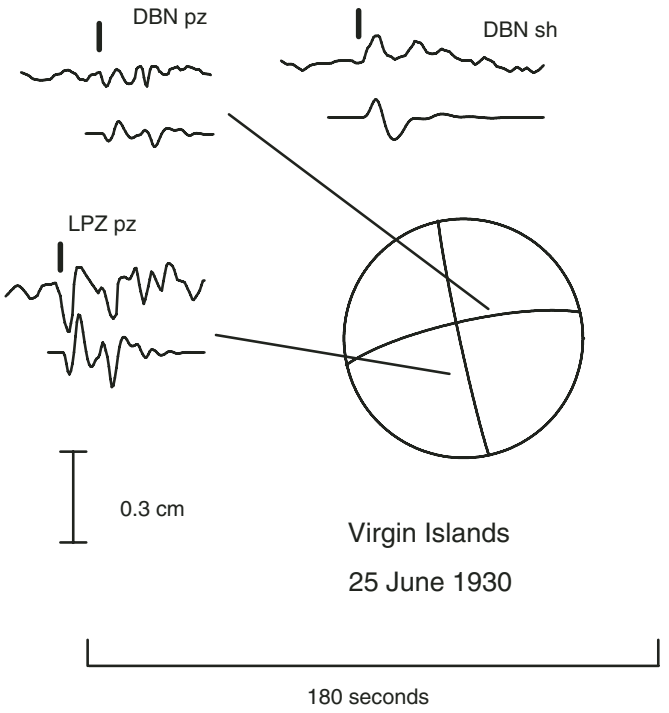

Figure A8. Results obtained from forward modeling of the 1930 Virgin Islands earthquake. DBN—DeBilt, Netherlands; LPZ—La Paz, Bolivia.

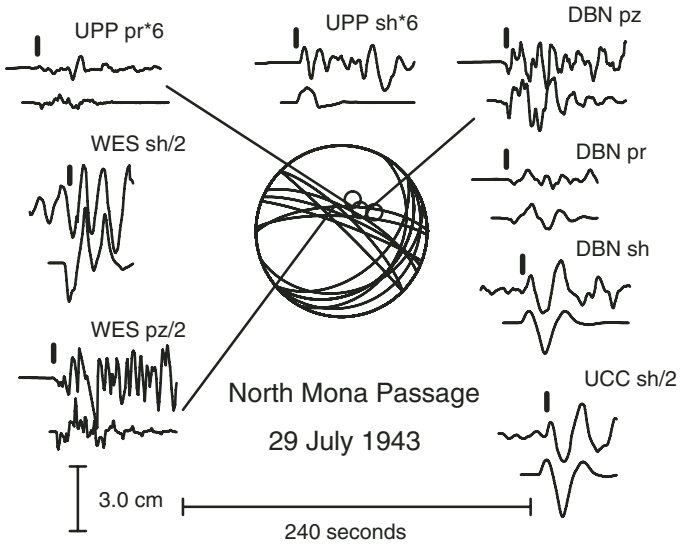

Figure A10. Waveform inversion results for the 1943 North Mona Passage earthquake. Open symbols indicate dilatations obtained from listings of the International Seismological Summary. DBN—DeBilt, Netherlands; UPP—Uppsala, Sweden; WES—Weston, Massachusetts.

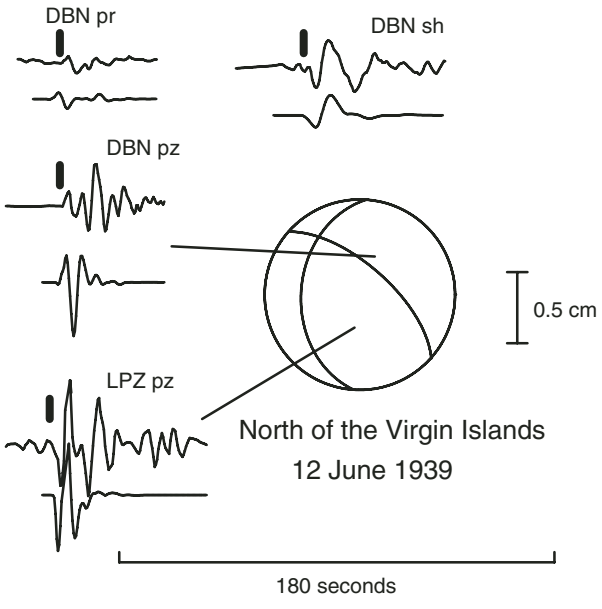

Figure A9. Results obtained from forward modeling of an earthquake located north of the Virgin Islands. This earthquake appears to be an outer rise event (see Fig. 8). DBN—DeBilt, Netherlands; LPZ—La Paz, Bolivia.

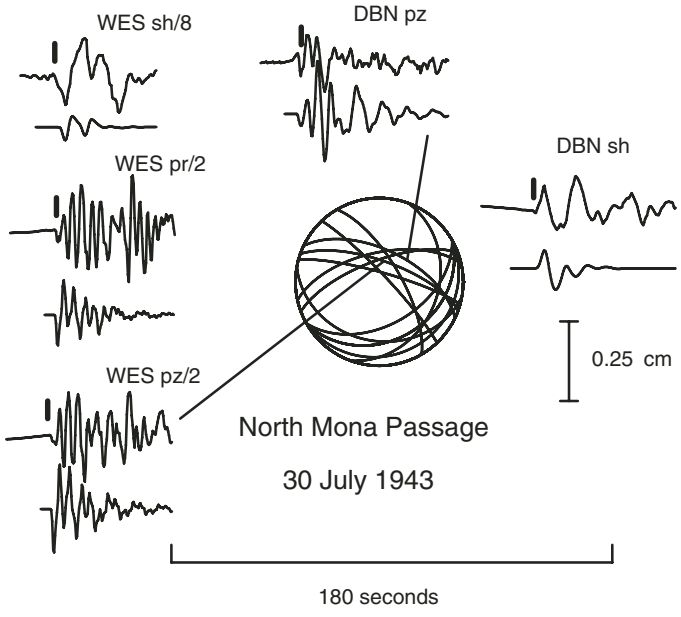

Figure A11. Waveform inversion results for an aftershock of the North Mona Passage earthquake. DBN—DeBilt, Netherlands; WES—Weston, Massachusetts.

ACKNOWLEDGMENTS

We thank seismograph station operators from around the world for sending us copies of the seismograms and instrument response information used in this study. Helpful reviews by J. Dewey, A. Villaseñor, and P. Mann greatly improved the manuscript. We thank C. von Hillebrandt-Andrade for her helpful discussions and comments during the early stages of this research. She pointed us toward many useful references. Discussions and information from P. Jansma and G. Mattioli are appreciated. Funding from the U.S. Geological Survey's Earthquake Hazards Reduction Program (00HQGR0013) is also acknowledged. The views and conclusions contained in this document are those of the authors and should not be interpreted as necessarily representing the official policies, either expressed or implied, of the U.S. Government.

REFERENCES CITED

Baker, M.R., and Doser, D.I., 1988, Joint inversion of regional and teleseismic waveforms: Journal of Geophysical Research, v. 93, p. 2037–2045.

Coffman, J.L., and von Hake, C.A., 1982, Earthquake History of the United States: Boulder, Colorado, U.S. Department of Commerce, National Oceanic and Atmospheric Administration publication 41-1, 258 p.

Deng, J., and Sykes, L.R., 1995, Determination of Euler pole for contemporary relative motion of Caribbean and North America plates using slip vectors of interplate earthquakes: Tectonics, v. 14, p. 39–53, doi: 10.1029/94TC02547.

Dillon, W.P., Edgar, N.T., Scanlon, K.M., and Coleman, D.R., 1994, A review of the tectonic problems of the strike-slip northern boundary of the Caribbean Plate and examination by GLORIA, *in* Gardner, J.V., Field, M.E., and Twichell, D.C., eds., Geology of the United States' seafloor: The view from GLORIA: Cambridge, Cambridge University Press, p. 135–164.

Dolan, J.F., and Wald, D.J., 1998, The 1943–1953 north-central Caribbean earthquakes: active tectonic setting, seismic hazards and implications for Caribbean-North American plate motions, *in* Dolan, J., and Mann, P., eds., Active strike-slip and collisional tectonics of the Northern Caribbean plate boundary zone: Geological Society of America Special Paper 326, p. 143–161.

Dolan, J.F., Mullins, H.T., and Wald, D.J., 1998. Active tectonics of the north-central Caribbean: Oblique collision, strain partitioning, and opposing subducted slabs, *in* Dolan, J., and Mann, P., eds., Active strike-slip and collisional tectonics of the Northern Caribbean plate boundary zone: Geological Society of America Special Paper 326, p. 1–63.

Doser, D.I., and Webb, T.H., 2003, Source parameters of large historical (1917–1961) earthquakes: North Island, New Zealand, v. 152, p. 795–832.

Doser, D.I., Webb, T.H., and Maunder, D.E., 1999, Source parameters of historic (1918–1962) earthquakes, South Island, New Zealand: Geophysical Journal International, v. 139, p. 769–794, doi: 10.1046/j.1365-246x.1999.00986.x.

Gutenberg, B., and Richter, C.H., 1954, Seismicity of the Earth and associated phenomena: New York, Hafner Publishing Company, 245 p.

Huerfano, V., 1995, Crustal structure and stress regime near Puerto Rico [M.S. thesis]: Mayaguëz, University of Puerto Rico.

Jansma, P.E., Mattioli, G.S., Lopez, A., DeMets, C., Dixon, T.H., Mann, P., and Calais, E., 2000, Neotectonics of Puerto Rico and the Virgin Islands, northeastern Caribbean, from GPS geodesy: Tectonics, v. 19, p. 1021–1037, doi: 10.1029/1999TC001170.

Larue, D.K., and Ryan, H.F., 1990, Extensional tectonism in the Mona Passage, Puerto Rico and Hispaniola: A preliminary study: Transactions of the 12th Caribbean Geological Conference, p. 310–313.

Mann, P., Calais, E., Ruegg, J.-C., DeMets, C., Jansma, P.E., and Mattioli, G.S., 2002, Oblique collision in the northeastern Caribbean from GPS measurements and geological observations: Tectonics, v. 21, no. 6, p. 1057, doi: 10.1029/2001TC001304.

Masson, D.G., and Scanlon, K.M., 1991, The neotectonic setting of Puerto Rico: Geological Society of America Bulletin, v. 103, p. 144–154, doi: 10.1130/0016-7606(1991)103<0144:TNSOPR>2.3.CO;2.

McCann, W.R., 1985, On the earthquake hazards of Puerto Rico and the Virgin Islands: Bulletin of the Seismological Society of America, v. 75, p. 251–262.

McCann, W.R., and Sykes, L.R., 1984, Subduction of aseismic ridges beneath the Caribbean plate: implications for the tectonics and seismic potential of the northeastern Caribbean: Journal of Geophysical Research, v. 89, p. 4493–4519.

Mercado, A., and McCann, W., 1998, Numerical simulation of the 1918 Puerto Rico tsunami: Natural Hazards, v. 18, p. 57–76, doi: 10.1023/A:1008091910209.

Molnar, P., and Sykes, L., 1969, Tectonics of the Caribbean and Middle American regions from focal mechanisms and seismicity: Geological Society of America Bulletin, v. 80, p. 1639–1684.

Petroy, D.E., and Wiens, D.A., 1989, Historical seismicity and implications for a diffuse plate convergence in the NE Indian Ocean: Journal of Geophysical Research, v. 94, p. 12,301–12,319.

Reid, H.F., and Taber, S., 1919, The Porto Rico earthquakes of October–November 1918: Bulletin of the Seismological Society of America, v. 9, p. 95–127.

Russo, R.M., and Bareford, C., 1993. Historical seismicity of the Caribbean region, 1933–1963, Caribbean Conference on Volcanism, Seismicity, and Earthquake Engineering, Trinidad, October 1993: University of the West Indies.

Russo, R.M., and Villaseñor, A., 1995, The 1946 Hispaniola earthquakes and the tectonics of the North America–Caribbean plate boundary zone, northeastern Hispaniola: Journal of Geophysical Research, v. 100, p. 6265–6280, doi: 10.1029/94JB02599.

Russo, R.M., Okal, E.A., and Rowley, K.C., 1992, Historical seismicity of the southeastern Caribbean and tectonic implications: Pure and Applied Geophysics, v. 139, p. 87–120.

Soto-Cordero, L., and Bataille, K., 1993, Study of seismicity and stress patterns in the southwestern part of the Puerto Rico trench: Eos (Transactions, American Geophysical Union), v. 74, p. 418.

van Gestel, J.P., Mann, P., Dolan, J., and Grindlay, N., 1998, Structure and tectonics of the upper Cenozoic Puerto Rico–Virgin Islands carbonate platform as determined from seismic reflection studies: Journal of Geophysical Research, v. 103, p. 30,505–30,530, doi: 10.1029/98JB02341.

Wysession, M.E., Okal, E.A., and Miller, K.L., 1991, Intraplate seismicity of the Pacific basin: Pure and Applied Geophysics, v. 135, p. 261–359.

Manuscript Accepted by the Society August 18, 2004

Geological Society of America Special Papers

Historical earthquakes of the Puerto Rico–Virgin Islands region (1915–1963)

Diane I. Doser, Christina M. Rodriguez and Claudia Flores

Geological Society of America Special Papers 2005;385; 103-114
doi:10.1130/0-8137-2385-X.103

Notes